analytical chemistry

pubs.acs.org/ac Article

Plasmon-Enhanced Bimodal Nanosensors: An Enzyme-Free Signal Amplification Strategy for Ultrasensitive Detection of Pathogens

Nilamben Panchal, Vedant Jain, Rebekah Elliott, Zachary Flint, Paul Worsley, Caine Duran, Tuhina Banerjee,* and Santimukul Santra*

Cite This: *Anal. Chem.* 2022, 94, 13968−13977 Read Online

ACCESS | Metrics & More | Article Recommendations | Supporting Information

ABSTRACT: Increasing foodborne illnesses have led to global health and economic burdens. *E. coli* O157:H7 is one of the most common disease-provoking pathogens and known to be lethal Shiga toxin-producing *E. coli* (STEC) strains. With a low infection dose in addition to person-to-person transmission, STEC infections are easily spread. As a result, specific and rapid testing methods to identify foodborne pathogens are urgently needed. Nanozymes have emerged as enzyme-mimetic nanoparticles, demonstrating intrinsic catalytic activity that could allow for rapid, specific, and accurate pathogen identification in the agrifood industry. In this study, we developed a sensitive nanoplatform based on the traditional ELISA assay with the synergistic properties of gold and iron oxide nanozymes, replacing the conventional enzyme horseradish peroxidase (HRP). We designed an easily interchangeable sandwich ELISA composed of a novel, multifunctional magneto-plasmonic nanosensor (MPnS) with target antibodies (MPnS-Ab). Our experiments demonstrate a 100-fold increase in catalytic activity in comparison to HRP with observable color changes within 15 min. Results further indicate that the MPnS-Ab is highly specific for *E. coli* O157:H7. Additionally, effective translatability of catalytic activity of the MPnS technology in the lateral flow assay (LFA) platform is also demonstrated for *E. coli* O157:H7 detection. As nanozymes display more stability, tunable activity, and multi-functionality than natural enzymes, our platform could provide customizable, low-cost assay that combines high specificity with rapid detection for a variety of pathogens in a point-of-care setup.

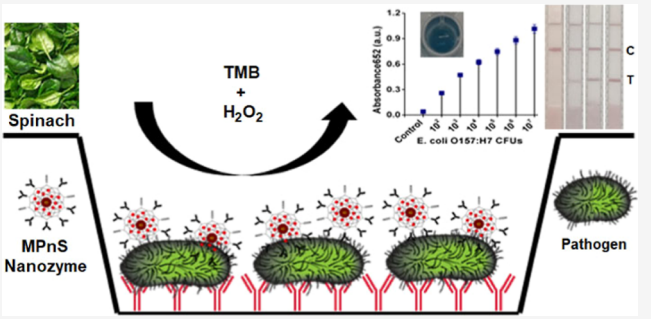

INTRODUCTION

Evidence indicates the foodborne outbreaks and resultant diseases in the United States are increasing.[1] With the Centers for Disease Control (CDC) estimating 48 million illnesses, 128,000 hospitalization, and 3000 deaths annually in the U.S.,[2] foodborne illnesses present a considerable health and economic burden. The most common method of transmission is consumption of contaminated food or water,[3] *Escherichia coli* (*E. coli*) plays a key role in infection[4] with some *E. coli* strains linked to foodborne illnesses in international scale outbreaks.[5] The most lethal strain, Shiga toxin-producing *E. coli* (STEC) serotype O157:H7, first emerged in the 1980s as a significant public health risk.[6] Despite vigilant oversight and regulations in most countries, produce-associated outbreaks are on the rise[7] with recent outbreaks worldwide having been traced to leafy salad greens.[8,9] The CDC in conjunction with the Federal Drug Administration (FDA) have yet to identify the source(s) of two *E. coli* O157:H7 infections, both found to be from STEC strains. In the past year, the United States confronted three highly publicized, multistate outbreaks.[10] The World Health Organization (WHO) recently published data attributing STEC as the cause of 1 million illnesses, 100 deaths, and 13,000 disability-adjusted life years.[11] Rapid spread is not surprising as STEC has a low infection dose of only 10−100 organisms and is passed through person-to-person contact.[8] The verotoxins expressed by STEC are known to be virulent to humans causing gastrointestinal disease worldwide, including bloody diarrhea, and hemorrhagic colitis and life-threatening hemolytic-uremic syndrome.[12−15] This is further concerning as the healthcare field confronts multidrug-resistant bacteria, of which drug-resistant strains of *E. coli* have proven to be transmittable to humans through direct and indirect contact with food and water.[16] This highlights the importance of rapid, accurate detection to quickly identify pathogens and reduce contamination and infection caused by ingestion of contaminated food or drinking sources.

In the past decades, new methods for disease detection have emerged. Iron oxide nanoparticles (IONPs) were considered to be inert until the intrinsic peroxidase-like properties of

Received: July 24, 2022
Accepted: September 12, 2022
Published: September 26, 2022

https://doi.org/10.1021/acs.analchem.2c03215
Anal. Chem. 2022, 94, 13968−13977

Fe_3O_4 were demonstrated in 2007, opening a new field of research combining nanotechnology with the biocatalytic activity of enzymes.[17] Due to the high catalytic activity and specificity, enzymes and biocatalysts have long been explored and utilized including in consumer, commercial, and clinical applications.[18−24] In the past decades, enzymes have become indispensable in agrifood detection with an increasing role in food safety issues due to their sensitivity and selectivity in detecting ions, small molecules, proteins, and both chemical and biological contaminants.[25,26] However, limitations have hindered advancement and use as natural enzymes function under relatively mild conditions.[27,28] Disadvantages of their use include high costs for preparation and purification, instability, easy denaturation, and challenges in recycling and reuse.[29,30] These drawbacks have led researchers to pursue artificial enzymes as low-cost and stable alternatives since the 1950s.[31,32] This led to the discovery of materials such as fullerenes, cyclodextrins, polymers, and dendrimers-based enzymes having similar structure and function.[33−39] However, concerns about biocompatibility and catalytic efficiency have hindered success.

The next generation of artificial enzymes are nanozymes, nanomaterial-based artificial enzymes. Significant research in this area has led to a new concept, nanozymology, combining nanotechnology with biology[40] and has ushered in a new era of enzyme-mimetic exploration. More than 300 types of nanomaterials with intrinsic enzymatic properties have now been discovered.[41] Nanozymes catalyze the same biocatalytic reactions as natural enzymes despite extreme pH and temperature, with the functional properties of enzyme mimics.[42] As a result, nanozymes have become increasingly popular for widespread use in agrifood detection of ions, small molecules, proteins, and biological contaminants.[43] Widespread implementation of nanozymes has also driven numerous biomedical advancements including immunoassays, biosensors, and antibacterial and antibiofilm agents.[44,45] Numerous nanomaterials have been investigated and discovered to have catalytic activities similar to peroxidase, oxidase, catalase, and superoxide dismutase enzymes.[46−51] Exhibiting the same oxidation function as horseradish peroxidase (HRP) and the basis for well-known ELISA assay, nanozymes are ideal for pathogen detection as they can bind with antibodies to detect analytes of interest.[52] Additionally, they exhibit multienzyme mimetic activity,[53] demonstrate enhanced stability and durability for lower production costs,[30,54,55] can be easily mass produced, display tunable activity, and have a large surface area for multi-functionalization.[41]

In this study, we exploit the multifunctionality of nanozymes in the form of a novel magneto-plasmonic nanosensor (MPnS) for rapid detection of *E. coli* O157:H7. The intrinsic peroxidase-like activity demonstrated by magnetic iron oxide (Fe_3O_4) nanoparticles (IONPs) combined with the enzymatic activity of gold nanoparticles (GNPs) was shown to work synergistically, resulting in a robust pathogen detection system based on colorimetric kinetics. GNPs were encapsulated in the polymer-coatings of IONPs using a one-step synthesis method, as described in the Supporting Information. Oxidation of 3,3′,5,5′-tetramethylbenzidine (TMB) provides a visual color change, demonstrating a range of intensities dependent on the anti-*E. coli* O157:H7 mAb concentration on the surface of MPnS. GNPs are recognized for their remarkable surface plasmon resonance (SPR) and display UV−vis property in addition to their catalytic activity. Our studies indicated that MPnS functioned 100-fold times more efficiently than HRP and could be used as a rapid, accurate, and customizable assay for detecting a wide variety of pathogens. In addition, this MPnS nanozyme technology was successfully adopted in the lateral flow assay (LFA) technology for the sensitive and timely detection of *E. coli* O157:H7 in the field.

EXPERIMENTAL SECTION

Peroxidase-Like Activity of Nanozymes. The enzymatic activity of nanozymes is dependent on the concentrations of H_2O_2, pH, size, and temperature. We measured the catalytic activity of nanozymes from 0 to 1 M H_2O_2 concentrations, 1.0 to 9.0 pH, 20 to 60 °C, and nanozymes with varying sizes. The TMB concentration was kept constant, 800 μM. We compared the relative enzymatic activity of GNPs, IONPs, and MPnS varying those parameters and evaluated the findings in comparison with the natural enzyme HRP. A high-throughput plate-reader was used to measure the reaction at 652 nm wavelength.

Kinetic Analysis. Catalytic activity of HRP, IONPs, GNPs, and MPnS was determined at room temperature in 4.5 mL cuvettes using 20 pM HRP, 0.9 pM IONPs, 0.6 pM GNPs, and 0.2 pM MPnS in the presence of 10 mM of H_2O_2 for HRP and 950 mM of H_2O_2 for nanozymes, with TMB added as a substrate. As the TMB concentration was increased, the nanozyme activity also increased, resulting in a non-linear curve. A Michaelis−Menten graph was obtained using Origin Pro 2019 with the Michaelis−Menten enzyme kinetic model and Levenberg Marquardt iteration graph. All reactions were measured using a Genesys 150 spectrophotometer with kinetics method at 652 nm. The maximum initial velocity (V_{max}), Michaelis−Menten constant (K_m), and catalytic constant (k_{cat}) were determined for HRP and nanozymes using $k_{cat} = V_{max}/[E]$ equation, where $[E]$ is the enzyme concentration.

Optimization of the Antibody Concentration for Passive Conjugation. The pH of GNPs and MPnS were adjusted at 9.0 using 0.1 M potassium carbonate buffer. 250 μL of MPnS solution (O.D. = 1.0) was added in different concentrations of antibodies (0, 0.5, 1, 2, 4, 6, 8, and 15 μg/mL) and incubated for 10 min. Then, 50 μL of 10% NaCl solution was added to 50 μL of MPnS-Ab conjugates and incubated for 10 min. Absorbance at 580 nm was measured and the value plotted against antibody concentrations. IONPs were conjugated using our previously reported protocol.[56]

Sandwich Immunoassay. The 96-well microplate was coated with 200 μL of anti-*E. coli* O157:H7 capture antibody (0.1 mg/mL) in coating buffer and incubated overnight at 4 °C. After incubation, the microplate was rinsed three times with a washing buffer (PBS, 1X, pH 7.4), leaving the layer of capture antibody undisturbed. Blocking buffer was then added to the wells for 2 h at 37 °C and then rinsed three times with washing buffer. In each well, different colony forming units (CFUs) of *E. coli* O157:H7 (0−10^8 CFUs) were added and incubated for 2 h at 37 °C. Unbound bacterial CFUs were removed by rinsing the plates with washing buffer three times. MPnS-Ab {100 μL, [Fe] = 1.0 mM, [Antibody] = 8 μg/mL} were added to each well and allowed to incubate for 2 h at room temperature. The wells were again rinsed three times with washing buffer. 100 μL of PBS (1X, 7.4 pH), 800 μM TMB, and 950 mM H_2O_2 were then added to each well and incubated for 10 min. Absorbance was measured using a high-throughput plate-reader (λ_{abs} = 652 nm), and photographs

https://doi.org/10.1021/acs.analchem.2c03215
Anal. Chem. 2022, 94, 13968−13977

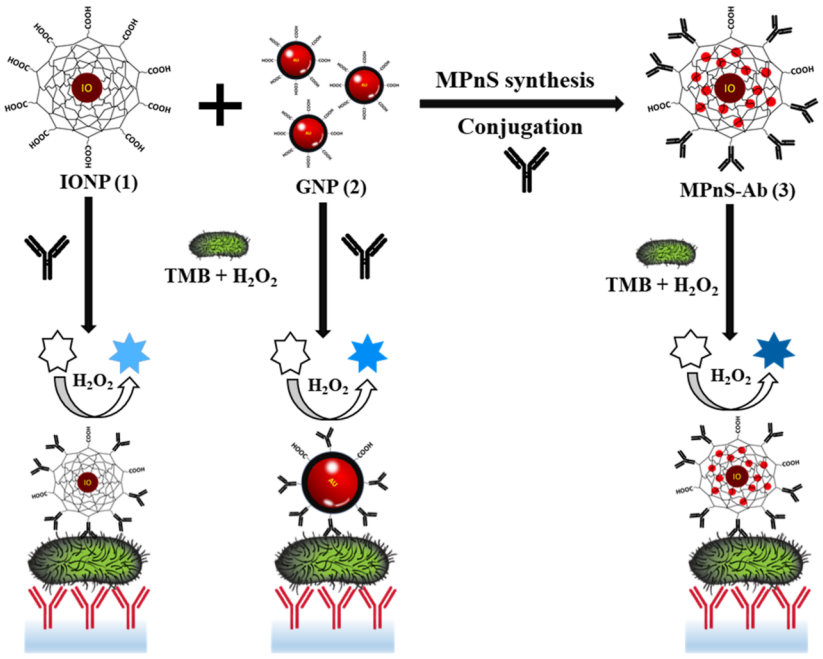

Figure 1. Schematic illustration of nanozyme-mediated sandwich ELISA. Synthesis of antibody-conjugated functional MPnS and its working principle for the detection of *E. coli* O157:H7.

were taken with an iPhone. Similarly, GNP and IONP conjugate-based ELISA assays were performed and compared with HRP-based conventional ELISA.

Specificity Assay. For the confirmation of specificity, sandwich ELISA experiments were performed using 10^7 CFUs of two different strains of bacteria: *E. coli* O157:H7, *E. coli* O111, and *S. typhimurium*, and a mixed culture containing all three pathogens. The capture and detection antibodies were specific to *E. coli* O157:H7; therefore, findings were analyzed to determine the specificity based on minimum to no binding with the other pathogens. Similar protocols were used for the time-dependent assays.

Sandwich ELISA in Complex Food Matrices. Detection of pathogens in complex food matrices using MPnS-Ab {[Fe] = 1.0 mM, [Antibody] = 8 μg/mL} in milk and spinach rinse were performed. A sterile stomacher bag was used to prepare spinach rinse, where spinach leaves and 1X PBS (equal weight) were gently mixed for 10 min. Milk (2% in 1X PBS) and spinach rinse were spiked with *E. coli* O157:H7 and diluted to the final desired CFUs (10^2–10^8) in each sample. Next, similar protocols were followed for *E. coli* O157:H7 detection, as previously used for sandwich immunoassay.

Analytical Performance of MPnS-Ab Nanozyme: Wet Conjugate Testing for LFA Experiments. The analytical sensitivity of MPnS and antibody passive conjugation were analyzed using LFA strips. The detection of *E. coli* O157:H7 was carried out using different concentrations of antibodies (0–15 μg/mL) conjugated on MPnS. The *E. coli* O157:H7 CFUs were kept constant at 10^6. In a 96-well plate, 40 μL of reaction buffer containing 150 mM Tris-HCL pH 8, 1% BSA, and 0.1% Triton X-100 were incubated with 20 μL of *E. coli* O157:H7 (10^6 CFUs). Next, 20 μL of MPnS-Ab conjugates {[Fe] = 1.0 mM, [Antibody] = 0–15 μg/mL} was added and mixed with pipette, and the LFA strip was inserted vertically. After 10 min, images were captured and lines intensity quantified using ImageJ software.

Field-Based Detection of *E. coli* O157:H7 Using MPnS-Ab in the LFA Format. The sample solution was prepared by adding 20 μL of different CFUs (10^3–10^7) of *E. coli* O157:H7 diluted in 1X PBS (pH 7.4) to 40 μL of reaction buffer containing 150 mM Tris-HCL pH 8, 1% BSA, and 0.1% Triton X-100 in a 96-well plate. 20 μL of MPnS-Ab {[Fe] = 1.0 mM, [Antibody] = 8.0 μg/mL} was added, and the solution was mixed with pipette. The LFA strip was inserted vertically in a 96-well plate. After 10 min, images were taken with an iPhone camera, and the intensity of lines were quantified using ImageJ software.

RESULTS AND DISCUSSION

Syntheses of Nanozymes, IONPs, GNPs, MPnS, and Their Conjugates. In this study, we propose a novel strategy for the synthesis of MPnS composed of IONPs and GNPs and to investigate its intrinsic peroxidase activity (Figure 1). The facile MPnS synthesis approach is significantly different from the conventional strategies, which involves two distinct steps: polyacrylic acid (PAA)-coated IONP preparation[57] (4 mM, T2 = 100–110 ms, Supporting Information, Figure S1), *in situ* GNP formation using an optimized Turkevich method[58] ($HAuCl_4$, 5 mM; citrate solution, 0.5%; Supporting Information, Figure S2), and simultaneous encapsulation in IONP's PAA coatings in one step. The successful completion of Au^{+3} reduction was marked by the appearance of darkish ruby red color (λ_{max} = 522 nm, Figure 2), which was also used for the assessment of endpoint for MPnS synthesis. The stability of these nanozymes was assessed by measuring changes in diameters over a period of 60 days (Supporting Information, Figure S3), and the results are presented in Supporting Information (Table S1). The surface-exposed carboxylic acid groups of purified MPnS (2.0 mM) were functionalized with targeted anti-*E. coli* O157:H7 mAb using the conventional passive conjugation method. We hypothesized that combining IONPs with GNPs could result in synergistic interactions, enhancing the overall enzymatic properties of MPnS. We used

https://doi.org/10.1021/acs.analchem.2c03215
Anal. Chem. 2022, 94, 13968–13977

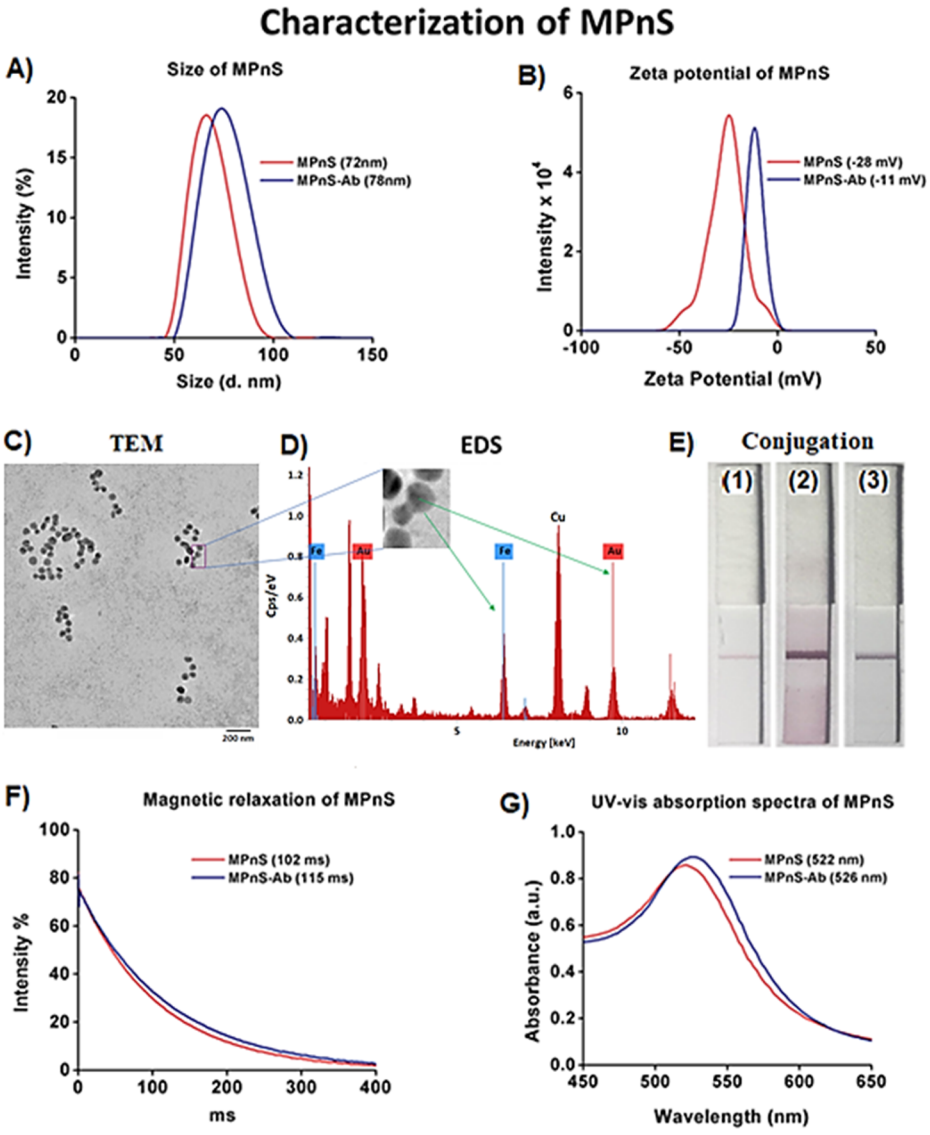

Figure 2. Characterization of MPnS and antibody-conjugated MPnS: (A) hydrodynamic radii of MPnS before and after conjugation, inset: image of MPnS and (B) ζ potential. (C) TEM, scale bar: 200 nm and (D) EDS of MPnS. (E) Images of the conjugation half strips, confirming for the successful antibody conjugation of (1) positive control, (2) on GNPs and (3) on MPnS. (F) T2 magnetic relaxation and (G) UV−vis absorption spectra of MPnS and MPnS-Ab, further confirming for successful conjugation.

the peroxidase-like activity of the synthesized enzyme-mimetics in colorimetric assay, which is dependent on the color change from clear to blue by oxidizing the peroxidase substrate TMB in the presence of H_2O_2. Higher the enzymatic efficiency results in a greater intensity in blue color. The antibody conjugation step was important for the formation of sandwich ELISA consisting of MPnS bound to TMB and the detection antibody, which in the presence of the target pathogen will undergo a redox reaction, leading to the observable color change. In addition, it operates on the basic principle that unbound antigens will be discarded in subsequent washes. Initial results showed that the most pronounced color change, a darker blue, was obtained with functional MPnS-Ab when compared with individual IONP-Ab and GNP-Ab. This led us to proceed with testing our hypothesis that MPnS could be used as rapid and highly specific colorimetric assay for pathogen detection.

Characterization Studies of MPnS and MPnS-Ab Conjugates. Following the successful synthesis and purification of MPnS and anti-*E. coli* O157:H7 mAb-conjugated MPnS (MPnS-Ab), detailed characterization experiments were performed using DLS, transmission electron microscopy (TEM), energy-dispersive X-ray spectroscopy (EDS), T2 MR, and UV−vis spectrometry. DLS experiments were performed to measure the average change in the particle size and ζ potential before and after conjugation of MPnS with antibody. The average hydrodynamic diameter of MPnS changed from 72 to 78 nm when conjugated with anti-*E. coli* O157:H7 mAb (Figure 2A). ζ potential further indicated successful conjugation showing an expected change in negative surface charge from −28 to −11 mV after conjugation (Figure 2B). The association of counter ions of neighboring water molecules on the negatively charged MPnS-Ab resulted in the relative increase in ζ potential. TEM experiments showed the formation of IO-Au composites in MPnS, which was further confirmed by EDS elemental analysis (Figure 2C,D). The successful conjugation of anti-*E. coli* O157:H7 antibody on the surface of MPnS was also confirmed using the conjugation kit

https://doi.org/10.1021/acs.analchem.2c03215
Anal. Chem. 2022, 94, 13968−13977

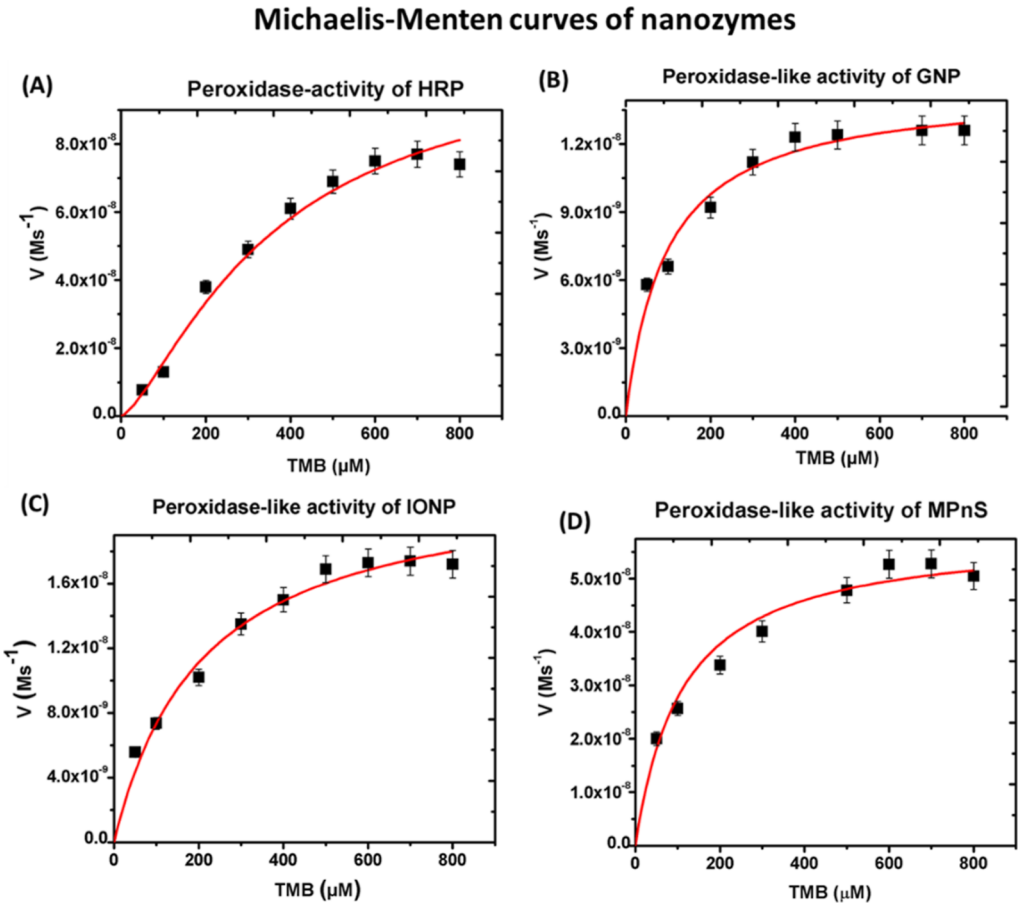

Figure 3. Kinetic parameters of nanozymes and natural enzyme HRP exhibiting peroxidase activity: steady-state kinetic analysis using the Michaelis−Menten model of (A) HRP, (B) GNPs, (C) IONPs, and (D) MPnS by varying TMB concentrations.

from Abcam. Appearance of a visible line on the protein A/G test strip indicated that the antibody was successfully conjugated on GNPs (2) and MPnS (3, Figure 2E). Additionally, we used the spin−spin T2 magnetic relaxation (MR) diagnostic technique, as explained in the previous literature.[59] In brief, binding of target analytes displaced water molecules, leading to measurable changes in the spin−spin magnetic relaxation time (ΔT2). This was observed with the MPnS measured at 102 ms and the MPnS-Ab increasing to 115 ms (Figure 2F). The next confirmation method used to evaluate the successful conjugation of Abs was the optical absorption by exploiting the SPR property of Au^0 in MPnS. UV−vis absorption spectra demonstrated that the conjugation reaction occurred with the unbound MPnS measured at 522 nm compared to MPnS-Ab at 526 nm (Figure 2G). The red shift in SPR indicated for the successful conjugation.

Next, we optimized the catalytic activity[60] of the synthesized nanozymes by varying specific important parameters including H_2O_2, pH, temperature, and size and compared with natural enzyme HRP, as demonstrated in Supporting Information (Figure S4). Results indicated that the nanozymes, specifically MPnS, is stable in harsher conditions and exhibited better catalytic activities compared to HRP and other nanozymes.

Peroxidase-Like Catalytic Activity of Nanozymes. With the wide variety of nanozyme applications continuing to emerge and their catalytic activity being dependent on physiochemical properties such as morphology, size, and composition, enzymatic activity and characterization of our MPnS were essential to this study. We based our protocol on a repeatable and reliable catalytic standard[40] to measure and define enzymatic activity using Michaelis−Menten kinetics (Figure 3). H_2O_2 concentrations were held constant at 950 mM, whereas TMB concentrations were increased to find V_{max}, the maximum reaction rate defined by substrate concentration saturation for GNPs, IONPs, and MPnS. For HRP, the H_2O_2 concentration was kept constant at 10 mM. While HRP showed the highest V_{max} at 8.7×10^{-8} M/s (Figure 3A) as expected, Michaelis−Menten kinetics demonstrated that each nanozyme outperformed HRP's catalytic activity (k_{cat}) (Figure 3B−D). K_m demonstrates how quickly the reaction increases with the substrate concentration (Table 1), an indication of substrate affinity. The lower the K_m, the higher the affinity. Our experiments indicate GNPs have the greatest affinity with the

Table 1. Kinetic Parameters of HRP, IONPs, GNPs, and MPnS Nanozymes Obtained from Michaelis−Menten Curves[a]

catalyst	K_m (μm)	V_{max} ($\times 10^{-8}$ M/s)	k_{cat} (s^{-1})
HRP	243	8.7	4.3×10^3
IONPs	208	2.3	2.5×10^4
GNPs	96	1.4	2.4×10^4
MPnS	111	5.9	5.9×10^5

[a] K_m denotes the Michaelis constant, and V_{max} is the maximum velocity. k_{cat} is the catalytic constant and is expressed by the formula $k_{cat} = V_{max}/[E]$, where $[E]$ is the total enzyme concentration.

https://doi.org/10.1021/acs.analchem.2c03215
Anal. Chem. 2022, 94, 13968−13977

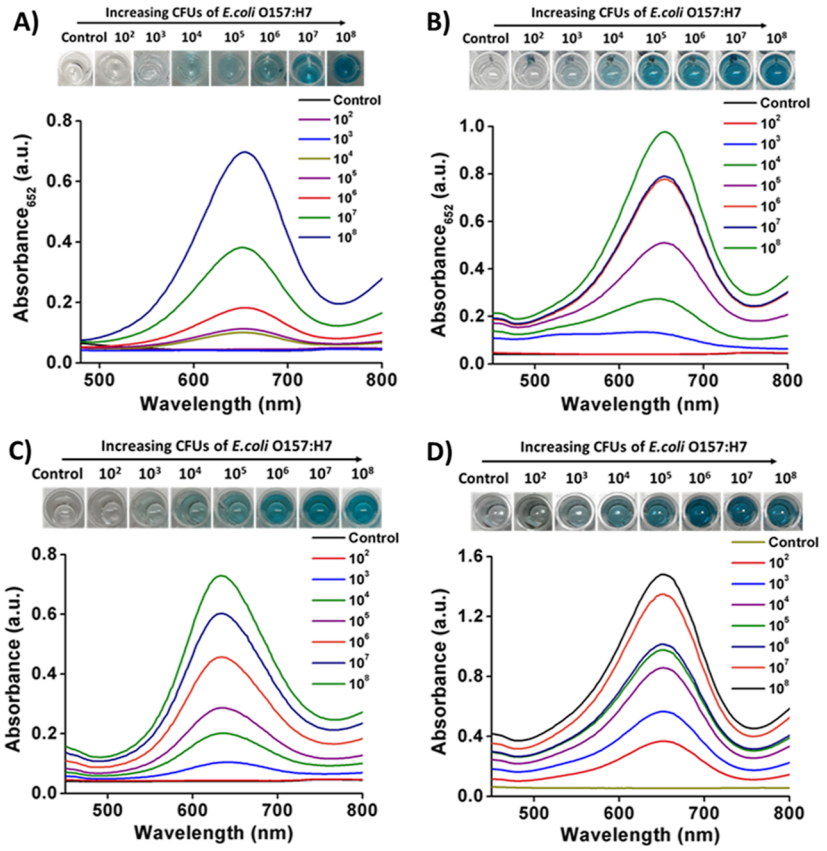

Figure 4. Colorimetric and SPR detections of different CFUs of *E. coli* O157:H7 spiked in 1X PBS using (A) HRP, (B) GNPs, (C) IONPs, and (D) MPnS in the conventional sandwich ELISA format. The absorbance of TMB at 652 nm is plotted as a function of different CFUs of *E. coli* O157:H7 bacteria.

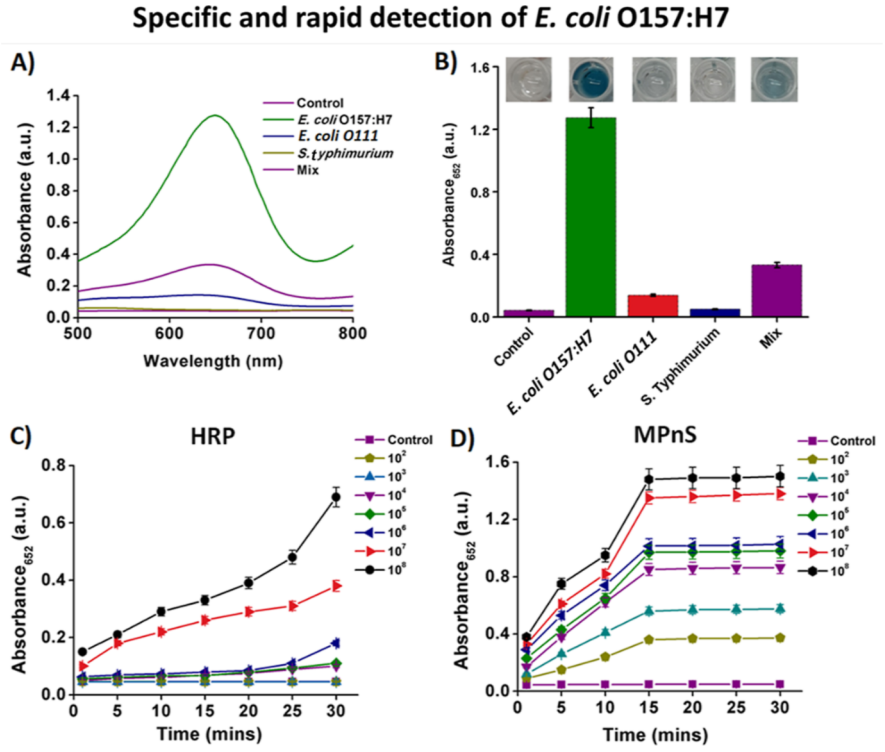

Figure 5. (A,B) Specificity of MPnS-Ab nanozyme was evaluated by conducting MPnS-based sandwich ELISA in the presence of other bacterial cross-contaminants and a mixture. Time-dependent *E. coli* O157:H7 detection assay using (C) HRP and (D) peroxidase-mimetic MPnS-Ab nanozyme.

https://doi.org/10.1021/acs.analchem.2c03215
Anal. Chem. 2022, 94, 13968−13977

K_m value at 96 μM. Each synthetic nanozyme demonstrated much greater affinity than HRP, which demonstrated the highest K_m at 243 μM. However, when measuring the catalytic constant, k_{cat}, representing the maximum number of substrate molecules converted to the product, we were surprised to see both GNPs and IONPs showed k_{cat} values to be 10-fold higher than HRP. Furthermore, our MPnS displayed the highest turnover number, with k_{cat} demonstrating a significant 100-fold difference at 5.9×10^5 in comparison to HRP at 4.3×10^3. We postulated that the IO-Au composite and negative ζ charges in our MPnS nanozyme resulted in good catalytic activity due to the positive charges of the substrate. This tremendous increase in enzymatic activity led us to hypothesize that a customizable sandwich ELISA using the MPnS could result in a successful and robust colorimetric pathogen detection system.

Peroxidase-Based Sandwich ELISA for the Detection of *E. coli* O157:H7. In order to determine the stabilizing concentration of anti-*E. coli* O157:H7 mAb for conjugation with MPnS {[Fe] = 1.0 mM}, flocculation experiments were performed using the protein A/G test strip (half-strip). As demonstrated in the Supporting Information, the functional MPnS conjugate synthesized with 8 μg/mL mAb concentration (Supporting Information, Figure S5) was found to be the most stable and selected for the ELISA experiments.

To demonstrate the superior peroxidase-mimetic activity in biosensing applications, we have applied the synthesized functional GNPs, IONPs, MPnS conjugates (1.0 mM), and HRP in the sandwich ELISA format (Figure 4). The absorbance of TMB was monitored at 652 nm, the absorbance maximum of oxidized TMB, to demonstrate the sensitivity of the natural and artificial enzymes with CFUs of *E. coli* O157:H7 (Supporting Information, Figure S6). The rate of oxidation in the sandwich ELISA coupling interaction with target bacteria was collected *via* colorimetric assay, observable by naked eyes and absorbance measurements. Color changes were increasing not noticeable with HRP until CFUs reached to the concentrations of 10^4, and then, color intensity gradually changed as the concentration increased (Figure 4A). Notably, the GNP and IONP nanozymes showed observable differences in color and increase in absorbance at a CFU concentration of 10^3 (Figure 4B,C). On the other hand, MPnS exhibited a 100-fold increase in the detection sensitivity as predicted by the kinetic studies, showing an observable difference in color and absorbance at a CFU concentration of 10^2 (Figure 4D). There was also a marked difference in color intensity when comparing HRP to all three nanozymes as bacterial concentrations increased. In addition, to visually compare the detection sensitivities of nanozymes with HRP (Supporting Information, Table S2) and to provide a side-by-side absorbance differences, Supporting Information Figure S7 indicates that our MPnS can be used as a highly sensitive detection assay for *E. coli* O157:H7.

Specific and Rapid Detection of *E. coli* O157:H7. To address the robust detection capability of functional MPnS nanozyme, we used UV absorbance and colorimetry sandwich ELISA assays to demonstrate higher specificity for *E. coli* O157:H7 in the presence of other pathogenic contaminants, including *S. typhimurium* and another *E. coli* strain, specifically *E. coli* O111 (10^7 CFUs, Figure 5A,B). While the interaction of *S. typhimurium* was almost as minimum as the control, *E. coli* O111 demonstrated slight reactivity with the MPnS-Ab {[Fe] = 1.0 mM, [Antibody] = 8 μg/mL} but not enough to be visible to the naked eye. However, high specificity for *E. coli* O157:H7 was demonstrated with an intense color change, which was also clearly observed by UV absorbance.

In addition to the specificity, we performed time-dependent assays to demonstrate that our nanozyme platform can be used for rapid testing of *E. coli* O157:H7. We first analyzed with HRP, which requires higher bacterial concentrations and showed optimal function with CFUs magnitude of 10^7 and detection signals beyond 30 min (Figure 5C). This was expected as HRP is used in the traditional ELISA assay where it starts to visually change in color at around 20 to 30 min. When compared, the peroxidase-mimetic MPnS demonstrated detection capabilities beginning at concentrations as low as 10^2–10^3 CFUs with a detection time of 15 min (Figure 5D). We reasoned that the synergistic effects of GNPs and IONPs enhanced the sensitivity, resulting in quicker readings with a stable signal within 10 to 15 min and improving upon the standard ELISA assay. This further confirms that our MPnS trimodal detection system could be used onsite for real-time, sensitive, and rapid detection of *E. coli* O157:H7.

Detection of *E. coli* O157:H7 in Complex Food Matrices. To further demonstrate the real-world and field-deployable detection capability of our MPnS-based sandwich ELISA colorimetric assay in the agrifood industry, *E. coli* O157:H7 recoveries were detected in real-world complex food samples, including milk and spinach rinse (Figure 6A,B). While

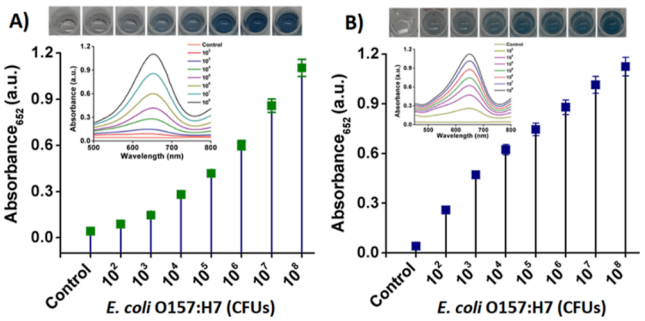

Figure 6. Colorimetric and SPR detection of different CFUs of *E. coli* O157:H7 spiked in (A) milk and (B) spinach rinse using MPnS nanozyme in the sandwich ELISA format. The absorbance of TMB at 652 nm is plotted as a function of different CFUs of bacteria.

sensitivity was slightly lessened in the milk sample due to presence of milk-based higher-molecular-weight protein interferences, yet the bacterial CFUs were detected in concentrations as low as 10^3. However, MPnS {[Fe] = 1.0 mM, [Antibody] = 8 μg/mL} showed comparatively higher sensitivity, detecting CFUs at concentrations of 10^2 in spiked spinach samples. This may be due to the presence of lower-molecular-weight natural product interferences from spinach rinse. These sensitive detection analyses further confirm our hypothesis that the MPnS nanozyme can be effectively used to detect *E. coli* O157:H7 at low concentration levels in field applications. This result is significant due to the low infection rate of this bacteria in food and drinking sources. Furthermore, due to the adaptability of our platform, MPnS-based sandwich ELISA assay could easily be customized to detect a variety of pathogens.

Implication of MPnS Nanozyme in LFA for Field-Based *E. coli* O157:H7 Detection. To explore the potential application of the MPnS-Ab nanozyme platform in the conventional LFA format for the field-based detection of *E. coli* O157:H7, we have performed two separate sets of

https://doi.org/10.1021/acs.analchem.2c03215
Anal. Chem. 2022, 94, 13968−13977

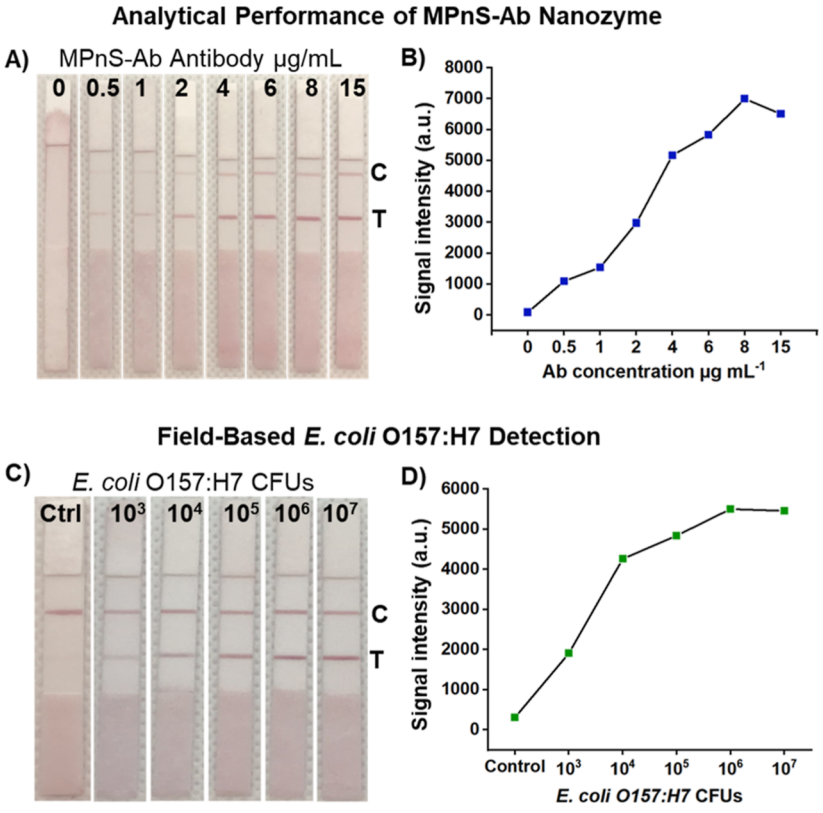

Figure 7. (A) Assessment of analytical sensitivity of MPnS-Ab conjugates by measuring the binding of 10^6 CFUs of *E. coli* O157:H7 to the control (***C***) and test (***T***) lines. (B) Quantification of test line intensities using ImageJ software. (C) Representative images of the test strips after applying different concentrations of the bacteria. (D) Quantification of the signal intensities of the test line (***T***) indicates visual limit of detection 10^3 CFUs of *E. coli* O157:H7.

experiments. (1) In the first set of experiments, the analytical performance of MPnS-Ab conjugates {[Fe] = 1.0 mM} was assessed based on the binding efficiency to the control (***C***) and the test (***T***) lines of lateral flow test strips using fixed 10^6 CFUs of *E. coli* O157:H7. Figure 7A shows the efficient binding response of MPnS-Ab conjugates on LFA strips. The results of the LFA test strips were imaged using a smartphone and analyzed using ImageJ software. Based on the color intensities of the test (***T***) and control (***C***) lines (Figure 7B), once again, the optimum anti-*E. coli* O157:H7 mAb concentration of 8.0 μg/mL was identified to be used for further studies. (2) Once the optimized MPnS-Ab conjugate was identified {[Fe] = 1.0 mM, [Antibody] = 8 μg/mL} based on its analytical sensitivity, it was applied in the LFA test format for the detection of different CFUs of *E. coli* O157:H7 (103−107). LFA detection results with different CFUs of *E. coli* O157:H7 on test strips are presented in Figure 7C. The visual detection limit obtained using the MPnS-Ab conjugate was about ∼10^3 CFUs with assay time of 10 min. Signal intensities of the test lines (***T***) were plotted against each CFU concentration of *E. coli* O157:H7, as shown in Figure 7D using ImageJ software. Based on these findings, it was concluded that MPnS-Ab carrying plasmonic labels can also be utilized in similar fashion to GNP-based LFA test assays but with higher detection sensitivity. Ongoing LFA experiments are underway to explore the detection sensitivity of MPnS-Ab for the detection of *E. coli* O157:H7 in complex food matrices.

CONCLUSIONS

In summary, we have demonstrated a new approach for the successful synthesis of MPnS with integrated plasmonic and peroxidase-mimetic properties. The integration of GNPs and IONPs inside MPnS was characterized by TEM, EDS, T2 MR, and UV−vis spectroscopic experiments. The enhanced stability and superior peroxidase-like activity of MPnS nanozyme were observed when compared with natural enzyme HRP and other standalone nanozymes GNPs and IONPs. The flocculation study indicated for the formulation of stable MPnS-Ab when conjugated with 8 μg/mL anti-*E. coli* O157:H7 antibody and showed high specificity for the detection of *E. coli* O157:H7. Our results suggest that the superior catalytic activity of MPnS (k_{cat} ∼ 5.9 × 10^5 s^{-1}) was due to the synergistic peroxidase-mimetic activity of iron oxide and several encapsulated GNPs. In addition, kinetic studies showed the MPnS displays 100-fold increase in the *E. coli* O157:H7 detection sensitivity, when compared with natural enzyme. However, the sensitivity was found to be slightly compromised when detected in complex food matrices, including milk and spinach rinse, and may be due to the presence of interfering proteins and natural products. Due to the higher sensitivity and stability, the detection was rapid, and sandwich ELISA assay can be completed within 15 min, which is 30 min in the case of HRP-based detection. In addition, initial experiments have demonstrated that this new MPnS-Ab platform could be successfully used in the LFA format for field-based *E. coli* O157:H7 detection by applying its plasmonic properties with higher sensitivity. Taken together, our functional MPnS can greatly enhance the ability to detect bacterial contaminants in

https://doi.org/10.1021/acs.analchem.2c03215
Anal. Chem. 2022, 94, 13968−13977

simple and complex food matrices in the early stages, which would markedly improve patient hospitalization and mortality rates. Future studies will further look into the translatability of catalytic activity of the MPnS technology in the LFA platform for field-based detection of *E. coli* O157:H7 in complex food matrices.

■ ASSOCIATED CONTENT

Supporting Information

The Supporting Information is available free of charge at https://pubs.acs.org/doi/10.1021/acs.analchem.2c03215.

Materials and instrumentations; detailed synthesis and characterization data for IONP, GNP, and MPnS nanozymes; stability studies of nanozymes; catalytic activity optimization; flocculation study for conjugation optimization; bacterial culture; and sandwich ELISA and LFA for *E.coli* O157:H7 detection (PDF)

■ AUTHOR INFORMATION

Corresponding Authors

Tuhina Banerjee − *Department of Chemistry and Biochemistry, Missouri State University, Springfield, Missouri 65897, United States*; Email: tbanerjee@missouristate.edu

Santimukul Santra − *Department of Chemistry, Pittsburg State University, Pittsburg, Kansas 66762, United States*; orcid.org/0000-0002-5047-5245; Email: ssantra@pittstate.edu

Authors

Nilamben Panchal − *Department of Chemistry, Pittsburg State University, Pittsburg, Kansas 66762, United States*

Vedant Jain − *Department of Chemistry, Pittsburg State University, Pittsburg, Kansas 66762, United States*

Rebekah Elliott − *Department of Chemistry, Pittsburg State University, Pittsburg, Kansas 66762, United States*

Zachary Flint − *Department of Chemistry and Biochemistry, Missouri State University, Springfield, Missouri 65897, United States*

Paul Worsley − *Department of Chemistry, Pittsburg State University, Pittsburg, Kansas 66762, United States*

Caine Duran − *Department of Chemistry, Pittsburg State University, Pittsburg, Kansas 66762, United States*

Complete contact information is available at: https://pubs.acs.org/10.1021/acs.analchem.2c03215

Notes

The authors declare no competing financial interest.

■ ACKNOWLEDGMENTS

This project was supported by the United States Department of Agriculture (USDA), ID: 2018-07295 to S.S. and T.B., and Kansas INBRE bridging grant (K-INBRE P20 GM103418) to S.S. This work was also supported by the MSU start-up fund to T.B. The authors would like to thank Lisa Whitworth and Oklahoma State University at Stillwater for the help with TEM and EDS experiments.

■ REFERENCES

(1) Centers for Disease Control and Prevention. (n.d.). *Preliminary Incidence and Trends of Infections with Pathogens Transmitted Commonly through Food—Foodborne Diseases Active Surveillance Network, 10 U.S. Sites, 2015−2018*; CDC. Retrieved January 25, 2021, from. https://www.cdc.gov/mmwr/volumes/68/wr/mm6816a2.htm?s_cid=mm6816a2_w.

(2) *Estimates of Foodborne Illness in the United States*; CDC, (2019). https://www.cdc.gov/foodborneburden/index.html.

(3) Byrne, L.; Jenkins, C.; Launders, N.; Elson, R.; Adak, G. K. *Epidemiol. Infect.* **2015**, *143*, 3475−3487.

(4) Nyachuba, D. G. *Nutr. Rev.* **2010**, *68*, 257−269.

(5) Beuchat, L. R. *J. Food Prot.* **1996**, *59*, 204−216.

(6) Adams, N. L.; Byrne, L.; Smith, G. A.; Elson, R.; Harris, J. P.; Salmon, R.; Smith, R.; O'Brien, S. J.; Adak, G. K.; Jenkins, C. *Emerg. Infect. Dis.* **2016**, *22*, 590−597.

(7) Jung, Y.; Jang, H.; Matthews, K. R. *Microb.Biotechnol.* **2014**, *7*, 517−527.

(8) Mikhail, A. F. W.; Jenkins, C.; Dallman, T. J.; Inns, T.; Douglas, A.; Martín, A. I. C.; Fox, A.; Cleary, P.; Elson, R.; Hawker, J. *Epidemiol. Infect.* **2018**, *146*, 1879.

(9) Centers for Disease Control and Prevention. *Outbreak of E. coli Infections Linked to Leafy Greens*, 2021. Available from:. https://www.cdc.gov/ecoli/2020/o157h7-10-20b/index.html. Accessed January 25.

(10) U.S Food and Drug Administration. Outbreak Investigation of E. coli O157:H7: Unknown Food (Fall 2020). Available from:. https://www.fda.gov/food/outbreaks-foodborne-illness/outbreak-investigation-e-coli-o157h7-unknown-food-fall-2020 (accessed on January 25, 2021).

(11) Pires, S. M.; Majowicz, S.; Gill, A.; Devleesschauwer, B. *Epidemiol. Infect.* **2019**, *147*, No. e236.

(12) Griffin, P. M.; Tauxe, R. V. *Epidemiol. Rev.* **1991**, *13*, 60−98.

(13) Gyles, C. L. *Can. J. Microbiol.* **1992**, *38*, 734−746.

(14) Ito, H.; Terai, A.; Kurazono, H.; Takeda, Y.; Nishibuchi, M. *Microb. Pathog.* **1990**, *8*, 47−60.

(15) Wang, G.; Clark, C. G.; Rodgers, F. G. *J. Clin. Microbiol.* **2002**, *40*, 3613−3619.

(16) Reinthaler, F. F.; Galler, H.; Feierl, G.; Haas, D.; Leitner, E.; Mascher, F.; Melkes, A.; Posch, J.; Pertschy, B.; Winter, I.; Himmel, W.; Marth, E.; Zarfel, G. *J. Water Health* **2012**, *11*, 13−20.

(17) Gao, L.; Zhuang, J.; Nie, L.; Zhang, J.; Zhang, Y.; Gu, N.; Wang, T.; Feng, J.; Yang, D.; Perrett, S.; Yan, X. *Nat. Nanotechnol.* **2007**, *2*, 577−583.

(18) Sun, H.; Zhang, H.; Ang, E. L.; Zhao, H. *Bioorg. Med. Chem.* **2018**, *26*, 1275−1284.

(19) Patel, R. N. *Bioorg. Med. Chem.* **2018**, *26*, 1252−1274.

(20) Huisman, G. W.; Collier, S. J. *Curr. Opin. Chem. Biol.* **2013**, *17*, 284−292.

(21) Panesar, P. S.; Kumari, S.; Panesar, R. *Crit. Rev. Biotechnol.* **2012**, *33*, 345−364.

(22) Fernandes, P. *Enzym. Res.* **2010**, *2010*, 1−19.

(23) Akoh, C. C.; Chang, S. W.; Lee, G. C.; Shaw, J. F. *J. Agric. Food Chem.* **2008**, *56*, 10445−10451.

(24) Kapoor, S.; Rafiq, A.; Sharma, S. *Crit. Rev. Food Sci. Nutr* **2015**, *57*, 2321−2329.

(25) Hemalatha, T.; UmaMaheswari, T.; Krithiga, G.; Sankaranarayanan, P.; Puvanakrishnan, R. *Indian J. Exp. Biol.* **2013**, *51*, 777−788.

(26) *Handbook of Food Safety Engineering*; Sun, D. W., Ed.; Wiley-Blackwell, 2011. https://doi.org/10.1002/9781444355321.

(27) Huang, L.; Sun, D.; Pu, H.; Wei, Q. *Compr. Rev. Food Sci. Food Saf.* **2019**, *18*, 1496−1513.

(28) Meunier, B.; de Visser, S. P.; Shaik, S. *Chem. Rev.* **2004**, *104*, 3947−3980.

(29) Kirby, A. J. *Acc. Chem. Res.* **1997**, *30*, 290−296.

(30) Wang, X. Y.; Guo, W. J.; Hu, Y. H.; Wu, J. J.; Wei, H. *Nanozymes: Next Wave of Artificial Enzymes*; Springer, 2016.

(31) Yan, X. Y. *Prog. Biochem. Biophys.* **2018**, *45*, 101−104.

(32) Breslow, R. *Artificial Enzymes*; Wiley-VCH: Weinheim, 2005.

(33) Ali, S. S.; Hardt, J. I.; Quick, K. L.; Sook Kim-Han, J.; Erlanger, B. F.; Huang, T.; Epstein, C. J.; Dugan, L. L. *Free Radic. Biol. Med.* **2004**, *37*, 1191−1202.

(34) Kataky, R.; Morgan, E. *Biosens. Bioelectron.* **2003**, *18*, 1407−1417.

(35) Kirkorian, K.; Ellis, A.; Twyman, L. J. *Chem. Soc. Rev.* **2012**, *41*, 6138−6159.
(36) Liu, L.; Breslow, R. *J. Chem. Soc.* **2003**, *125*, 12110−12111.
(37) Anderson, H. L.; Sanders, J. K. M. *J. Chem. Soc., Perkin Trans.* **1995**, *18*, 2223−2229.
(38) Romanovsky, B. V. *Macromol. Symp.* **1994**, *80*, 185−192.
(39) Gong, L.; Zhao, Z.; Lv, Y. F.; Huan, S. Y.; Fu, T.; Zhang, X. B.; Shen, G. L.; Yu, R. Q. *Chem. Commun.* **2015**, *51*, 979−995.
(40) Jiang, B.; Duan, D.; Gao, L.; Zhou, M.; Fan, K.; Tang, Y.; Xi, J.; Bi, Y.; Tong, Z.; Gao, G. F.; Xie, N.; Tang, A.; Nie, G.; Liang, M.; Yan, X. *Nat. Protoc.* **2018**, *13*, 1506−1520.
(41) Wang, P.; Wang, T.; Hong, J.; Yan, X.; Liang, M. *Front. Bioeng. Biotechnol.* **2020**, *8*, 15.
(42) Huang, Y.; Ren, J.; Qu, X. *Chem. Rev.* **2019**, *119*, 4357−4412.
(43) Huang, L.; Sun, D.; Pu, H.; Wei, Q. *Compr. Rev. Food Sci. Food Saf.* **2019**, *18*, 1496−1513.
(44) Wang, X.; Hu, Y.; Wei, H. *Inorg. Chem. Front.* **2016**, *3*, 41−60.
(45) He, W.; Wamer, W.; Xia, Q.; Yin, J.; Fu, P. P. *J. Environ. Sci. Health* **2014**, *32*, 186−211.
(46) Karakoti, A.; Singh, S.; Dowding, J. M.; Seal, S.; Self, W. T. *Chem. Soc. Rev.* **2010**, *39*, 4422−4432.
(47) Pirmohamed, T.; Dowding, J. M.; Singh, S.; Wasserman, B.; Heckert, E.; Karakoti, A. S.; King, J. E. S.; Seal, S.; Self, W. T. *Chem. Commun.* **2010**, *46*, 2736−2738.
(48) Singh, S. *Biointerphases* **2016**, *11*, 04B202.
(49) Karim, Md. N.; Anderson, S. R.; Singh, S.; Ramanathan, R.; Bansal, V. *Biosens. Bioelectron.* **2018**, *110*, 8−15.
(50) Zhang, H.; Liang, X.; Han, L.; Li, F. *Small* **2018**, *14*, 1803256.
(51) Zhao, M.; Tao, Y.; Huang, W.; He, Y. *Phys. Chem. Chem. Phys.* **2018**, *20*, 28644−28648.
(52) Singh, S. *Front. Chem.* **2019**, *7*, 46.
(53) Liang, M.; Yan, X. *Acc. Chem. Res.* **2019**, *52*, 2190−2200.
(54) Wei, H.; Wang, E. *Chem. Soc. Rev.* **2013**, *42*, 6060−6093.
(55) Wu, J.; Wang, X.; Wang, Q.; Lou, Z.; Li, S.; Zhu, Y.; Qin, L.; Wei, H. *Chem. Soc. Rev.* **2019**, *48*, 1004−1076.
(56) Banerjee, T.; Sulthana, S.; Shelby, T.; Heckert, B.; Jewell, J.; Woody, K.; Karimnia, V.; McAfee, J.; Santra, S. *ACS Infec. Dis.* **2016**, *2*, 667−673.
(57) Santra, S.; Kaittanis, C.; Grimm, J.; Perez, J. M. *Small* **2009**, *5*, 1862−1868.
(58) Kimling, J.; Maier, M.; Okenve, B.; Kotaidis, V.; Ballot, H.; Plech, A. *J. Phys. Chem. B* **2006**, *110*, 15700−15707.
(59) Banerjee, T.; Patel, T.; Pashchenko, O.; Elliott, R.; Santra, S. *ACS Appl. Bio Mater.* **2021**, *4*, 3786−3795.
(60) Xi, Z.; Gao, W.; Xia, X. *ChemBioChem* **2020**, *21*, 2440−2444.

https://doi.org/10.1021/acs.analchem.2c03215
Anal. Chem. 2022, 94, 13968−13977